Unclassified

SECURITY CLASSIFICATION OF THIS PAGE

...OCUMENTATION PAGE

Form Approved
OMB No 0704-0188

AD-A232 207

1b RESTRICTIVE MARKINGS

3 DISTRIBUTION/AVAILABILITY OF REPORT
Approved for public release; Distribution unlimited

4 PERFORMING ORGANIZATION REPORT NUMBER(S)
PL-TR-91-2022

5 MONITORING ORGANIZATION REPORT NUMBER(S)

6a NAME OF PERFORMING ORGANIZATION	6b OFFICE SYMBOL (If applicable)	7a NAME OF MONITORING ORGANIZATION
Phillips Laboratory, Geophysics Directorate	PHG	

6c ADDRESS (City, State, and ZIP Code)	7b ADDRESS (City, State, and ZIP Code)
Hanscom AFB Massachusetts 01731-5000	

8a NAME OF FUNDING/SPONSORING ORGANIZATION	8b OFFICE SYMBOL (If applicable)	9 PROCUREMENT INSTRUMENT IDENTIFICATION NUMBER

8c ADDRESS (City, State, and ZIP Code)	10 SOURCE OF FUNDING NUMBERS			
	PROGRAM ELEMENT NO	PROJECT NO	TASK NO	WORK UNIT ACCESSION NO
	61102F	2311	G5	01

11 TITLE (Include Security Classification)
Polar Cap Potentials and the Auroral Electrojet Indices

12 PERSONAL AUTHOR(S)
D.R. Weimer*, N.C. Maynard, W.J. Burke, C. Liebrecht**

13a TYPE OF REPORT	13b TIME COVERED	14 DATE OF REPORT (Year, Month, Day)	15 PAGE COUNT
Reprint	FROM _____ TO _____	1991 February 1	15

16 SUPPLEMENTARY NOTATION *Regis College Research Center, Weston MA 02193 (Now at: Geophysical Institute, University of Alaska, Fairbanks, Fairbanks AK 99775-0800) **ST Systems Corp., 4400 Forbes Blvd, Lanham MD 20706 - Reprinted from Planet Space Sci., Vol. 38 No. 9 pp1207-1222, 1990

17 COSATI CODES			18 SUBJECT TERMS (Continue on reverse if necessary and identify by block number)
FIELD	GROUP	SUB-GROUP	Auroral electric fields Electrojet currents

19 ABSTRACT (Continue on reverse if necessary and identify by block number)

Abstract—Electric potentials across the auroral zones and polar cap have been determined by an integration of electric fields measured on the Dynamics Explorer-2 satellite. Potentials from 527 cases, divided between winter and summer seasons in the northern hemisphere, are compared with simultaneous auroral electrojet indices which are measured with ground-based magnetic observatories. The dusk and dawn auroral potentials and the total polar cap potential are compared with the AU, AL, and AE indices respectively. The AE indices are found to be higher when it is summer in the northern hemisphere, due to the higher ionospheric conductivity. The electrojet currents are roughly proportional to the potentials, but the AE indices have a range of possible values for a given potential due to variations in the width and distribution of the electrojets, the ionospheric Hall conductivity, and the neutral wind velocity. The data have been fit to linear and non-linear equations, which may be used to estimate the potentials from the AE indices. Although the non-linear equations give slightly better fits than a straight line, the differences in the errors are not significant. Where possible the data have also been grouped according to the phase of magnetospheric substorms. These results indicate that substorms occur only when the polar cap potential exceeds a threshold of approximately 60 kV.

20 DISTRIBUTION/AVAILABILITY OF ABSTRACT	21 ABSTRACT SECURITY CLASSIFICATION
☐ UNCLASSIFIED/UNLIMITED ☒ SAME AS RPT ☐ DTIC USERS	Unclassified

22a NAME OF RESPONSIBLE INDIVIDUAL	22b TELEPHONE (Include Area Code)	22c OFFICE SYMBOL
N.C. Maynard	(617) 377-2431	PHG

DD Form 1473, JUN 86 *Previous editions are obsolete*

SECURITY CLASSIFICATION OF THIS PAGE
Unclassified

...Codes
...ail and/or
Special
A-1 20

Planet. Space Sci., Vol. 38, No. 9, pp. 1207–1222, 1990
Printed in Great Britain

0032-0633/90 $3.00 + 0.00

POLAR CAP POTENTIALS AND THE AURORAL ELECTROJET INDICES

D. R. WEIMER
Regis College Research Center, Weston, MA 02193
Now at: Geophysical Institute, University of Alaska Fairbanks, Fairbanks, AK 99775-0800

N. C. MAYNARD and W. J. BURKE
Geophysics Laboratory, Hanscom AFB, MA 01731

and

C. LIEBRECHT
ST Systems Corp., 4400 Forbes Blvd., Lanham, MD 20706

(Camera-ready copy received 25 July 1990)

Abstract—Electric potentials across the auroral zones and polar cap have been determined by an integration of electric fields measured on the Dynamics Explorer-2 satellite. Potentials from 527 cases, divided between winter and summer seasons in the northern hemisphere, are compared with simultaneous auroral electrojet indices which are measured with ground-based magnetic observatories. The dusk and dawn auroral potentials and the total polar cap potential are compared with the AU, AL, and AE indices respectively. The AE indices are found to be higher when it is summer in the northern hemisphere, due to the higher ionospheric conductivity. The electrojet currents are roughly proportional to the potentials, but the AE indices have a range of possible values for a given potential due to variations in the width and distribution of the electrojets, the ionospheric Hall conductivity, and the neutral wind velocity. The data have been fit to linear and non-linear equations, which may be used to estimate the potentials from the AE indices. Although the non-linear equations give slightly better fits than a straight line, the differences in the errors are not significant. Where possible the data have also been grouped according to the phase of magnetospheric substorms. These results indicate that substorms occur only when the polar cap potential exceeds a threshold of approximately 60 kV.

1. INTRODUCTION

In this paper we will show the results of a comparison of auroral and polar cap electric potentials and the Auroral Electrojet (AE) indices. The electric potential measurements are from the Vector Electric Field Instrument (VEFI) on the Dynamics Explorer-2 (DE-2) satellite. Potentials measured across the dawn and dusk auroral zones and the polar cap are compared with the AL, AU, and AE indices at the time of the satellite measurements.

There are several reasons why this comparison between potentials and AE indices can be useful. First of all, knowing how the potentials and electrojet currents relate to each other will promote an understanding of the electrodynamics of the aurora under both steady state and and substorm conditions. Secondly, although there have been studies of the relations between the interplanetary magnetic field (IMF) and the AE index and between the IMF and polar cap potential (in separate studies), there has never been an in-depth comparison between AE and potentials. With a functional relationship which is derived from simultaneous measurements of the potential by a satellite and the magnetic perturbations on the ground, it will be possible to estimate the potentials from the magnetic activity indices. This could be valuable to investigators who make use of the various electric field models; it would be useful to know if the total electric potential in a model is an accurate representation of the actual potential for a given level of magnetic activity. Also, if it can be determined how the potentials and electric fields relate to the AE indices, then it will be possible to improve estimates of the global ionospheric Joule heating as a function of the indices.

1.1. *The AE indices*

The Auroral Electrojet index was originally introduced by Davis and Sugiura (1966) as a measure of global electrojet activity in the auroral zone. The index is derived from the horizontal, northern component of geomagnetic variations observed at 10 to 13 observatories along the auroral zone in the northern hemisphere. The most positive value measured from all the stations is called the AU index and the

most negative value is the AL index. These names refer to the upper and lower envelopes of the overlapped plots of data from all stations. The AU and AL indices are understood to provide a measure of the respective eastward and westward electrojet currents at a given time. The difference between the AU and AL indices gives the AE index, which indicates the total maximum amplitude of the east and west electrojet currents. The mean value of AU and AL is the AO index.

The AU index is usually a positive number and the AL index is usually negative, but occasionally the largest horizontal variation (AU) is a negative number and at other times the smallest variation (AL) may be positive, due to contamination from the magnetospheric ring current or zonal currents in the ionosphere. However, the AE index by definition is always positive and is independent of zonal currents, although the physical meaning of the AE index is less obvious than that of of AU and AL indices taken separately (Mayaud, 1980).

The term "AE indices" is commonly used to refer to all four collective indices. These indices have advantages over the standard K_p indices in that they are an instantaneous measurement (i.e., one minute rather than three hour resolution) and have interpretable physical meaning (Davis and Sugiura, 1966). Presently the AE indices are calculated and distributed by the World Data Center C2 for Geomagnetism at Kyoto University.

1.2. *Theory*

At this point it is prudent to consider the physics which link satellite measurements of electric potential to the AE indices, in order to show that there is a valid reason for such a comparison. The potential is derived by an integration of the electric field which is measured by the satellite along it's direction of motion:

$$\Phi = \int_{w_1}^{w_2} E_x \, dx \, . \tag{1}$$

This potential is relative to the value at $x = w_1$. Assuming that the measured electric field is meridional (north-south), then there is a related Hall current in the azimuthal (east-west) direction:

$$J_H = \Sigma_H E_x \tag{2}$$

where Σ_H is the height-integrated Hall conductivity and J_H is the Hall current per unit length, integrated over the thickness of the ionosphere. The total Hall current is given by the integral of (2):

$$I_H = \Sigma_H \int_{w_1}^{w_2} E_x \, dx \tag{3}$$

where Σ_H has been assumed to be constant in the integration region. If w_1 and w_2 define the boundaries of the auroral zone (equatorward of the convection reversal) then the total auroral electrojet current, I_H, is proportional to the potential across the auroral zone:

$$I_H = \Sigma_H \Phi \, . \tag{4}$$

If Σ_H is not constant then the average value of the conductance in the region may be substituted as an approximation.

Since the AU index is related to the eastward electrojet, which tends to be located in the evening auroral zone (Davis and Sugiura, 1966) and is a Hall current driven by the northward electric field, then the AU index should be related to the potential across the evening aurora. Likewise, the AL index, which corresponds to the westward electrojet, should be related to the potential across the morning aurora. And since the polar cap potential is equal to the sum of the dusk and dawn potentials, and the AE index is equal to the sum of AU and AL (using absolute values), then these two quantities should be related. There is one serious problem with this reasoning, however. The AU/AL indices are not a measurement of the total electrojet currents, but are related

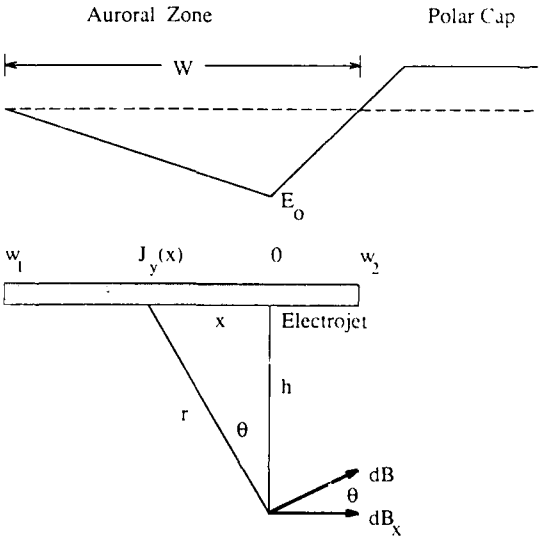

FIG. 1. SKETCH OF AN ASSUMED ELECTRIC FIELD AND ELECTROJET CURRENT DISTRIBUTION IN THE AURORAL ZONES. The electric field has a triangular distribution with peak magnitude E_o and width W. The Hall (electrojet) current has peak magnitude J_o at x=0. The electrojet current is at altitude h above the ground, where it causes a horizontal magnetic perturbation dB_x. The magnitude of the greatest horizontal perturbation is obtained by integrating the contribution due to $J_y(x)$ in the interval from $x=w_1$ to $x=w_2$.

to the maximum density of the electrojet current, as measured by the magnetic observatory which happens to be closest to the current maxima (Akasofu, 1989).

It is still possible to derive an approximate functional relationship between the potential and the peak measured ground magnetic perturbation if some assumptions are made about the distribution of the electric field and conductivity. We assume that the convection electric field in the auroral zone can be represented by a triangular function with width W and peak E_o, as shown in Figure 1, and the Hall conductivity is constant. The integrated electric field is:

$$\Phi = \frac{E_o W}{2} . \tag{5}$$

The horizontal, north-south magnetic field perturbation at the earth's surface will have its peak value directly below the location of the maximum Hall current. The total magnetic perturbation can be calculated by integrating the contributions from infinite-line currents of magnitude $J_y(x)$. Using the well-known formula for the magnetic field around an infinite wire,

$$B(r) = \frac{\mu_o J}{2\pi r} , \tag{6}$$

and the geometry shown in Figure 1, the total horizontal magnetic perturbation is

$$\Delta B_x = \frac{\mu_o}{2\pi} \int_{w_1}^{w_2} \frac{J_y(x) \cos\theta(x)}{r(x)} \, dx . \tag{7}$$

For the section of the electrojet extending from $x = 0$ (the location of the peak) to $x = w_1$, the integral is:

$$\Delta B_x = \frac{\mu_o J_o h}{2\pi} \int_0^{w_1} \frac{1 - \frac{x}{w_1}}{x^2 + h^2} \, dx \tag{8}$$

where J_o is the peak Hall current and h is the altitude of the electrojet above the ground. This integral evaluates to

$$\Delta B_x = \frac{\mu_o J_o f(R_1)}{2\pi} \tag{9}$$

with R_1 and $f(R)$ defined as

$$R_1 = \frac{w_1}{h} \tag{10}$$

$$f(R) = \arctan R - \frac{1}{2R} \ln(R^2 + 1) . \tag{11}$$

Adding the contribution for the integral from 0 to w_2 and doubling the result due to image earth currents, we arrive at

$$\Delta B_x = \frac{\mu_o J_o |f(R_1) + f(R_2)|}{\pi} . \tag{12}$$

Using (2) and (5), the final result is

$$\Delta B_x = \frac{2\mu_o \Sigma_H |f(R_1) + f(R_2)|}{W\pi} \Phi . \tag{13}$$

Since the altitude of the electrojet, h, is about 100 km, and the half-widths are in the range of 250 to 1,000 km, then R is in the range of 2.5 to 10, and $f(R)$ varies from 0.79 to 1.24; the function f is not very sensitive to the width or altitude of the electrojet. Equation 13 can be reduced to the form

$$\Delta B_x = c\Sigma_H \Phi . \tag{14}$$

The factor c is expected to vary from approximately 0.99 nT-ohm-kV^{-1} for W=2000 km to 2.54 nT-ohm-kV^{-1} for W=500 km.

In this analysis the Hall currents in the polar cap, which would reduce the magnitude of ΔB_x, have been neglected as these currents are usually too far away to have a significant effect. However, there is one more aspect to this problem which has more serious consequences: the electric field measured by the satellite (Equation 1) is in a co-rotating reference frame, while the electric field which determines the ionospheric currents (Equation 2) is in a frame relative to the neutral wind velocity. The neutrals are usually accelerated in the direction of $\mathbf{E} \times \mathbf{B}$ by drag forces (Killeen *et al.*, 1984). This has the effect of making the electrojet current smaller than what would be calculated from the measured potentials and the expected Hall conductivity. Lyons and Waltersheid (1986) have estimated that the neutrals will attain speeds of approximately 40% of the ion convection velocity, which would result in an "effective Hall conductivity" which is 60% of the actual Hall conductivity. Simultaneous measurements of ion-drift velocities and neutral wind velocities show that the relation between the two is complex and highly variable. Killeen *et al.* (1984) have found that at times the neutral and ion velocity vectors show agreement in both magnitude and direction, and at other times or locations there can be significant differences. They also found that the velocities in the dusk auroral zone tended to match better than in the dawn convection channel. The result of this complex ion-neutral relationship is to introduce additional variability into the relation between the magnetic field perturbations and the integrated potentials.

We also need to keep in mind that the actual measurements are subject to some errors which may upset the expected correlation. When the auroral oval contracts poleward at times of low activity many of the AE observatories will be well equatorward of the electrojet currents and will not make reliable measurements. And at times the satellite may measure a fraction of the full potential, since the orbit path might not cross the regions where the electric poten-

tial reaches its minimum and maximum values.

1.3. *Previous publications*

The theoretical relationship between the polar cap potential and ground magnetic perturbations had been considered by Crooker and Siscoe (1981), who used a two-ring model of the auroral zone and polar cap. However, their expression for the magnetic perturbations is given for a position equatorward of the auroral oval, rather than the maximum values (AE) within the oval. Right at the equatorward boundary, their Equation A17 reduces to:

$$\Delta B = \mu_o \Sigma_H \Phi \frac{a}{4b^2} \qquad (15)$$

where Φ is the total polar cap potential, a is the radius of the polar cap (inner radius of the auroral oval) and b is the outer radius of the auroral zone.

Another theoretical analysis has been done by Nisbet (1982), in which the relations between the Birkeland currents, Joule heating, and the AE indices are examined. Nisbet's Equation 34 for the relationship between the electric potential and AE indices is identical in form to our Equation 13. However, his expression (Equation 23) for the factor f is different, even though it is also based on a triangular distribution. (It appears that the $\cos\theta$ adjustment was omitted.) Nisbet did note that, since the polar cap potential shows less variation than the AL and AU indices, the variations in the electrojet indices are "mainly a response to Hall conductivity variations rather than to variations in the generator driving the Birkeland currents".

On the experimental side, the publications related to the present topic are much more numerous. Satellite measurements of electric potential across the polar cap are compared to solar wind parameters by Reiff *et al.* (1981), Wygant *et al.* (1983), and Doyle and Burke (1983). Reiff *et al.* (1981) had found that among the various indices of magnetic activity, the AE index had the highest correlation with polar cap potential, although the linear correlation was not as good as with the solar wind parameters. The best fit was found to be $\Phi(\mathrm{kV}) = 41 + 0.11\mathrm{AE(nT)}$. Since their primary purpose was to investigate the solar-wind coupling, this relation was not explored in any detail.

There have also been studies of the relationship between solar wind parameters and the AE indices by Perrault and Akasofu (1978), Meng *et al.* (1973), Baker *et al.* (1981), Bargatze *et al.* (1985), Tsurutani *et al.* (1985), and Sauvaud *et al.* (1987) (to name just a few). A common element in several of these papers is the finding that the best correlation between the AL index and IMF is found when the AL index is lagged by 40-60 minutes.

Various models for the distribution of the electric potential or plasma convection over the polar cap have been formulated, but these models have not been related to the AE indices. Empirical convection patterns have been derived by Foster *et al.* (1986) from radar observations; these patterns are keyed to "precipitation indices" which were derived from particle measurements on NOAA/TIROS weather satellites. A linear relationship was found between the polar cap potential and the precipitation index, which varies from 1 to 9. In another publication, Foster *et al.* (1989) have also calculated ionospheric conductances and field aligned currents for the same precipitation indices.

Heppner and Maynard (1987) had derived empirical convection models from DE-2 electric field data, keyed to various signs of z and y components of the interplanetary magnetic field. These models were drawn for moderately active conditions (K_p 3$^+$). Average cross polar cap potentials for different levels of K_p and AE were given and the expansion of the lower boundary with K_p was shown. Rich and Maynard (1989) put the Heppner-Maynard models into analytic form, with the magnitude of the polar cap potential depending on the K_p index. Ionospheric currents, joule heating, and field aligned currents were then calculated, using the analytic electric field models in combination with ionospheric conductivities which were based on a precipitation model by Hardy *et al.* (1987). This precipitation model is also based on K_p.

Spiro *et al.* (1982) have derived models for precipitating electron energy and auroral zone conductances which are parameterized according to the AE index. It was found that the AE index does a better job of ordering the data than other indices of geomagnetic activity. It would be useful to know how the electric potential varies according to the same index.

There have been many publications by Y. Kamide and associates about a method for calculating the distribution of currents and electric fields over the entire polar cap and auroral oval, through an "inversion" of the magnetic records from a number of stations in the northern hemisphere. Kamide and Baumjohann (1985) show both the total estimated electrojet currents and potential differences compared to the AU/AL indices. The ratio between the total westward electrojet and AL shows more variation than the eastward electrojet-AU ratio, particularly during substorms. They also observe that the ratio of the total electrojet current to the total potential difference increases during substorms. Kamide and Baumjohann (1985) conclude that the increase in the ionospheric current intensity prior to substorm onsets is due to an increase in the electric

field, and conductivity enhancements after onsets contribute to the maximum substorm currents. Ahn *et al.* (1989) make the same conclusion, also based on the Kamide method of inverting the ground-based magnetograms.

Ahn *et al.* (1984) have also used the inversion technique to compute polar cap potentials continuously for a two-day period in March, 1978. The derived potentials are then compared to the simultaneous AE indices. Their linear regression resulted in $\Phi(\mathrm{kV}) = 36 + 0.089\mathrm{AE}_{12}(\mathrm{nT})$ when 12-station magnetograms were used in the inversion. With more accurate 71-station computations the result was $\Phi(\mathrm{kV}) = 24 + 0.098\mathrm{AE}_{71}(\mathrm{nT})$. Baumjohann and Kamide (1984) used the same technique to derive a linear regression between total ionospheric Joule heating and the AE indices. However, their data shows a definite non-linear trend, which they did not fit due to the sparsity of data for high AE values. More recently, Richmond *et al.* (1990) have used the inversion technique combined with incoherent scatter radar observations from a two-day period in January, 1984. They found that $\Phi(\mathrm{kV}) = 22 + 0.119\mathrm{AE}_{12}(\mathrm{nT})$.

Ahn *et al.* (1983) derived empirical relations between ground magnetic disturbances and local ionospheric conductivities and electric fields, based on a comparison of data from one magnetic observatory and a nearby radar facility. The electric fields were related to the magnetic perturbations by power law equations, with different coefficients for positive and negative magnetic disturbances.

We've seen various parameters which have been related to the AE indices for limited time intervals. However, it is well known that the ionospheric conductivity changes with the season. Burch (1973) found seasonal variations in AU, but not in AL. Burch noted that this was consistent with the results of the conjugate point study of Meng and Akasofu (1968) which showed that the positive bays in the summer hemisphere were roughly twice those in the winter hemisphere, but there was no clear asymmetry for negative bays. Allen and Kroëhl (1975) also found significant, systematic seasonal AU intensity differences which average 60 nT between winter and summer. The AL values were not as clearly differentiated. Berthelier (1976) also saw seasonal effects in AE which were attributed to conductivity variations. There were also annual and diurnal variations in AE which Berthelier attributed to a shift of B_Z(GSM) relative to B_Z(GSE), which has a symmetrical distribution around a zero mean.

This synopsis of the literature indicates that a comprehensive, experimental comparison of AE indices and direct measurements of potential is still lacking. Furthermore, seasonal variations in ionospheric conductivity need to be taken into consideration.

2. OBSERVATIONS

2.1. *The DE-2 data set*

The DE-2 satellite was launched in August of 1981 into a 300 to 1000 km altitude polar orbit. The satellite reentered the atmosphere in March of 1983. Electric fields were measured on DE-2 by two orthogonal double probes in the orbit plane, with lengths of 22.4 m tip-to-tip. The data rate was 16 samples per second. Further details about the Vector Electric Field Instrument (VEFI) are given by Maynard *et al.* (1981).

Electric potentials are obtained by an integration of the measured electric fields along the satellite's path. For this study VEFI data were analyzed from 309 auroral/polar cap passes in the period from November 6, 1981 to January 4, 1982; and 218 passes in the period from May 1, 1982 to June 29, 1982. The data in the first period correspond to winter conditions in the northern hemisphere, and the second period correspond to summer conditions. The magnetic local times of the satellite's orbital track during these time periods was within about 3 hours of dawn and dusk (6 and 18 hours MLT). This restriction is given so that the satellite will have a reasonable chance of passing through the potential maximum and minimum of the typical two-cell convection pattern. The data used in this study do not include all that was obtained by the VEFI instrument during these time periods. There was some random selection of events due to circumstances of availability of processed data, and some passes were unsuitable for a measurement of the polar cap potential.

Electric fields measured with double probes are not without some uncertainty. "Contact potential" differences on the two probes can cause a small offset in the measured electric fields, which can lead to large errors in the potentials when integrated over long distances. To minimized these errors the contact potentials were adjusted for every polar pass in this study. Adjustments were made in such a way that the difference in integrated potential between the points of the pass at 45 degrees invariant latitude on each side of the pole was zero. In some cases the pass (when the instrument was turned on) started or ended at latitudes higher than 45 degrees. In those cases the beginning or end of the pass was used for the adjustment, provided that the electric field was still flat at that invariant latitude. If the beginning or the end of the pass was already inside the auroral zone then the pass was not used for this study.

The high latitude boundaries of the dawn and dusk

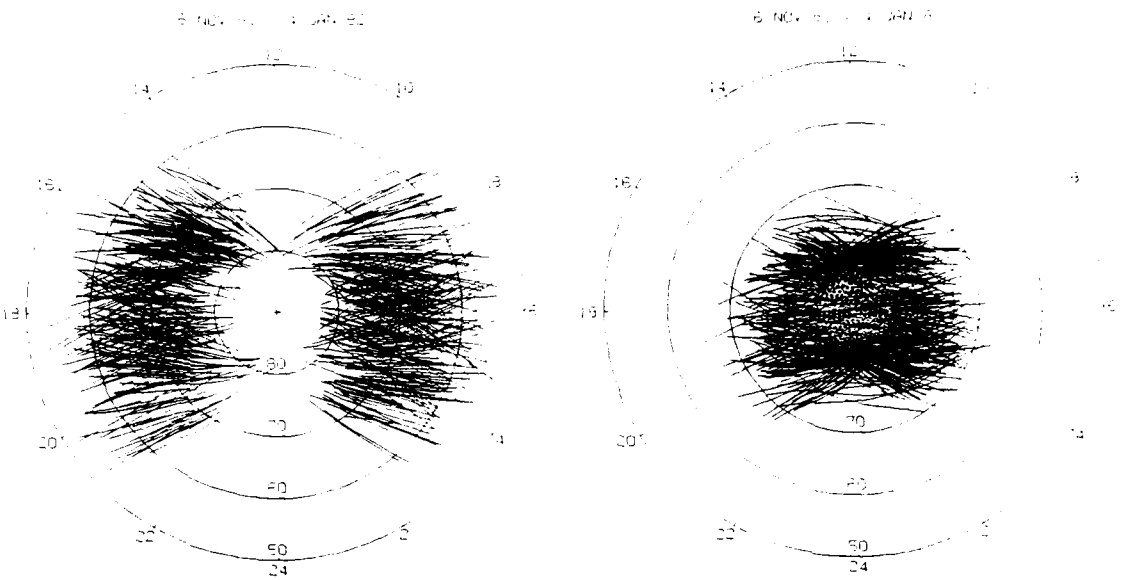

(a) (b)

FIG. 2. LOCATION OF THE PASSES BY THE DE-2 SATELLITE, IN MAGNETIC LOCAL TIME - INVARIANT LATITUDE COORDINATES, FOR THE PERIOD FROM 6 NOVEMBER, 1981 THROUGH 4 JANUARY, 1982. (a) Location of the dawn and dusk auroral zone passes. (b) Location of the polar cap passes

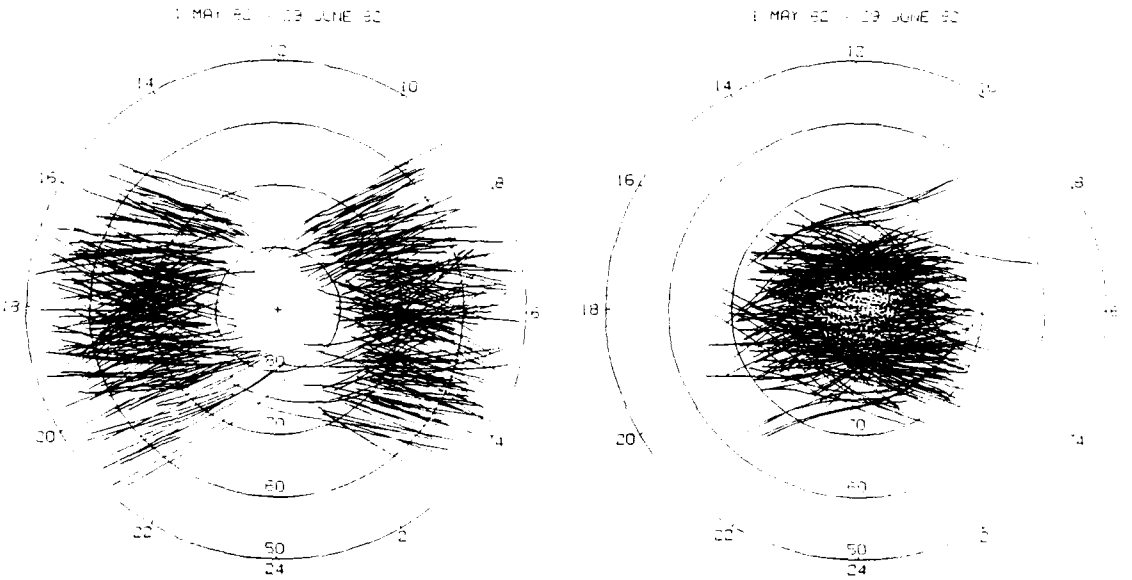

(a) (b)

FIG. 3. LOCATION OF THE PASSES BY THE DE-2 SATELLITE, IN MAGNETIC LOCAL TIME - INVARIANT LATITUDE COORDINATES, FOR THE PERIOD FROM 1 MAY, 1982 THROUGH 29 JUNE, 1982. (a) Location of the dawn and dusk auroral zone passes. (b) Location of the polar cap passes.

auroral zones were determined by the local maxima and minima of the integrated potential curves. The low latitude boundaries of the auroral zones were determined by choosing the points in which the electric field curve stopped being flat and rapid variations started. Figure 2a shows the locations of the dawn and dusk auroral zones derived from the electric field data for the winter period. This graph shows the orbit tracks of the DE-2 satellite between the low and high latitude auroral boundaries, in invariant latitude-MLT coordinates. In Figure 2b are shown the polar cap portions of the same passes. Figures 3a and 3b have the same format, but show the locations of the measurements during the summer period.

The difference between the potentials at the local maxima and minima gives the total polar cap potential. The difference between the potentials at the low and high latitude boundaries of the auroral zones gives the total potential across the dawn and dusk auroral zones. These relationships are illustrated in Figure 4, which shows an example of the electric field over the northern polar cap and the associated potentials.

2.2. *Comparison with AE Indices*

The AE indices with one minute time resolution were obtained on magnetic tape directly from the World Data Center C2 for Geomagnetism at Kyoto University. An average AU index was obtained for each dusk auroral zone crossing by averaging the one-minute AU indices corresponding to just the time period that the DE-2 satellite was in the dusk auroral zone, as determined by the electric field signatures. Likewise, an AL index was determined for each dawn auroral zone crossing, and an AE index was determined for each polar cap crossing. Thus, our comparisons are between simultaneous measurements.

Scatter plots of AU indices which are plotted in comparison with the dusk auroral potentials are shown in Figure 5. The signs of the dusk potentials, which are shown as negative numbers in Figure 4, have been reversed on this graph. There are separate plots for each of the two time periods. As mentioned earlier, one time period corresponds to winter in northern hemisphere and the other time period corresponds to summer in the northern hemisphere. The measurements which were made while DE-2 was in the northern hemisphere are marked with the crosses, and southern hemisphere passes are marked with the diamonds. Therefore the symbolic representation of the summer/winter "season" is reversed between the two plots, but the crosses consistently show potential measurements in the northern hemisphere, where the ground magnetic observatories are located.

There are three dashed lines drawn on each of these graphs. The lowermost dashed line shows a linear relationship between AU and the dusk potential, with the slope chosen such that 10% of the data points lie below the line and 90% of the points are above. Likewise, the uppermost dashed line shows the slope at which 10% of the points are above the line and 90% are below. These slopes bound the most likely range of the product "$c\Sigma_H$" in Equation 14. The middle dashed line shows the median slope, at which 50% of the points are above the line and 50% are below the line. The values of the 10%, 50%, and 90% slopes are given in Table 1.

In Figure 6 there are shown similar scatter plots for the AL indices and the simultaneous measurements of the dawn auroral potential. The signs of the AL indices have been reversed. Lines showing the 10%, 50%, and 90% slopes are also indicated on the figure.

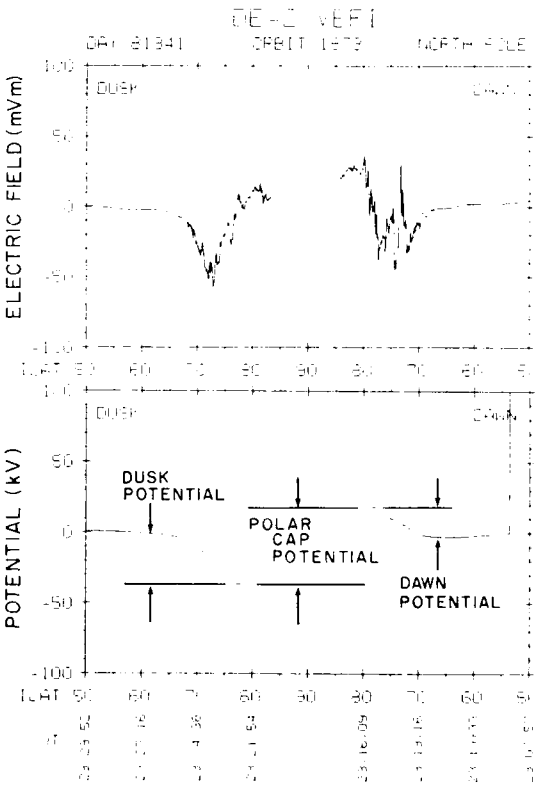

FIG. 4. EXAMPLE OF ELECTRIC FIELDS MEASURED BY THE VEFI INSTRUMENT ON DE-2 (upper panel) AND POTENTIALS OBTAINED BY INTEGRATING THE ELECTRIC FIELD (lower panel). The dusk and dawn potentials are defined as the difference between the potentials at the low and high latitude boundaries of the respective dusk and dawn auroral zones. The polar cap potential is defined as the difference between the potentials at the two high latitude boundaries, which are determined by the local minimum and maximum.

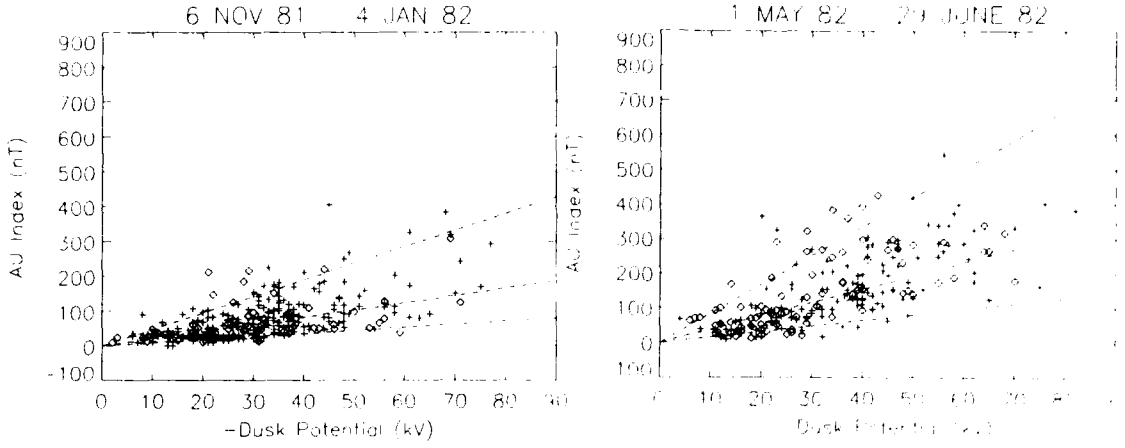

FIG. 5. SCATTER PLOT OF AU INDEX VS. -DUSK POTENTIAL. (a) Winter period in the northern hemisphere. (b) Summer period. The crosses mark the cases where the potential was measured in the northern hemisphere, and the diamonds show the southern hemisphere measurements. The dashed lines are at constant slopes which bound 10%, 50%, and 90% of the data points. The parameters for these lines are given in Table 1.

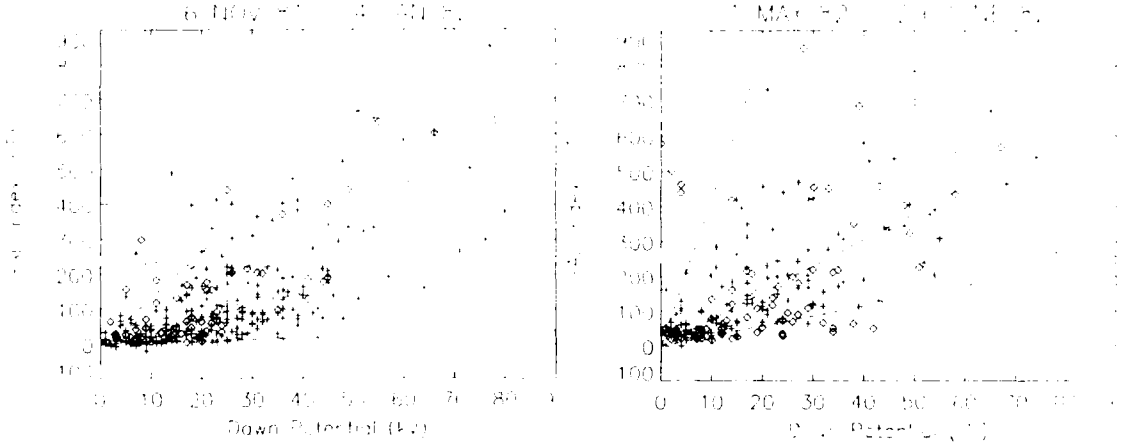

FIG. 6. SCATTER PLOT OF AL INDEX VS. DAWN POTENTIAL. (a) Winter period in the northern hemisphere. (b) Summer period. The format is the same as in Figure 5.

TABLE 1. SLOPES OF THE DASHED LINES ON FIGURES 5, 6, AND 7.

Data	Season	Figure	10% Slope	50% Slope	90% Slope
AU vs. $-\Phi_{Dusk}$	winter	5a	0.89	2.07	4.75
	summer	5b	1.61	3.86	8.38
AL vs. Φ_{Dawn}	winter	6a	0.43	3.65	13.13
	summer	6b	2.88	7.63	41.84
AE vs. Φ_{PC}	winter	7a	1.17	2.81	6.52
	summer	7b	2.34	4.95	9.62

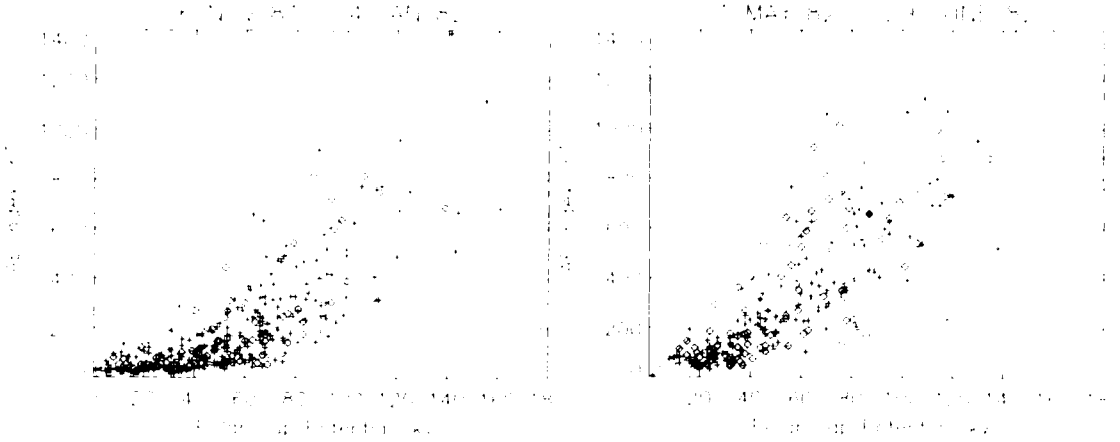

(a) (b)

FIG. 7. SCATTER PLOT OF AE INDEX VS. POLAR CAP POTENTIAL. (a) Winter period in the northern hemisphere. (b) Summer period. The format is the same as in Figure 5.

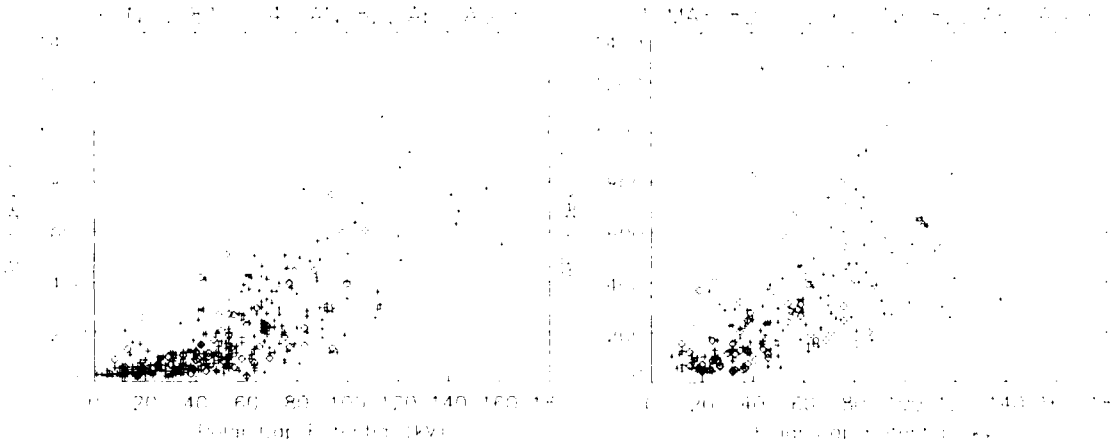

(a) (b)

FIG. 8. SCATTER PLOT OF AE INDEX VS. POLAR CAP POTENTIAL, WITH THE MEASUREMENT OF AE LAGGED 50 MINUTES BEHIND THE MIDDLE OF THE POLAR CAP CROSSING. (a) Winter period in the northern hemisphere. (b) Summer period.

and the values are included in Table 1. There are several points in Figure 6 which lie substantially above and to the left of the 90% slopes. Most likely this is because the satellite only measured a fraction of the full potential. Most of these abnormal potentials were measured in the winter hemisphere (plus symbol in Figure 5a and diamond symbols in Figure 6b), and at magnetic local times of 8 to 9 hours. At other local times there are no significant differences between the potentials in the northern and southern hemispheres.

Figure 7 shows the results of comparing the AE indices to the polar cap potentials, with the same format as in Figures 5 and 6. Similarly, the constants which describe the superimposed lines are in Table 1. The change in the ordinate axis is due to the fact that AE is by definition always positive, whereas AU and AL may have either sign.

We emphasize that the polar cap potentials and AE indices which are shown in Figure 7 are simultaneous. It had previously been shown that the polar cap potential is related to the IMF (Reiff *et al.*,

1981), and it had also been shown that the best correlation between the IMF and AE is obtained when AE is lagged by 40 to 60 minutes (Baker *et al.*, 1981; Bargatze *et al.*, 1985). Therefore, we have asked the question about whether or not a delay of 50 minutes between the polar cap potential measurements and the AE measurements would reduce the scatter in the data points. The answer, shown in Figure 8, is that the scatter is made worse by lagging the AE measurement behind the potential measurement by 50 minutes.

Since geomagnetic substorms by definition do cause large deviations in the AE index, the next step is to determine if the location of data points on the scatter graphs is related to substorm phase. For all 527 cases used in this study the charts of the AE, which are published by the World Data Center C2 for Geomagnetism, were examined to see if the satellite measurements took place during a well defined substorm "growth phase", "expansion phase", or "recovery phase". In many cases an unambiguous phase could not be identified. For the points where the phase was clear, the results are shown in Figures 9 and 10. The results indicate that the substorm phase does indeed influence the location of points on the graphs.

3. DISCUSSION

The results shown here indicate that, as expected, the relationships between the AE indices and the measured auroral polar cap potentials depends on the time of the year. The AE indices are larger in magnitude when it is summer in the northern hemisphere, where they are measured, due to the greater ionospheric conductivity (Allen and Kroehl, 1975). This is evident in the upward shift in the distribution of the AE indices between Figures 7a and 7b. There was also a downward shift in the distribution of the measured polar cap potential between the two time periods, which can be attributed to a lower sunspot number in June 1982 compared to December 1981. For the cases where IMF measurements are available we have also found that the distribution of B_Z(GSM) had changed to more northward, which accounts for the decreased polar cap potentials.

In the graphs which have been shown here the data have been separated according to the season in the northern hemisphere, where the magnetic observatories are located. This gives a more uniform grouping of the data points, in comparison to graphs (not shown) which group the data according to the season local to the satellite's potential measurements (i.e., combining the November January, northern hemisphere passes with the May June, southern hemisphere passes).

It is expected that the electric potential should be the same over the northern and southern polar caps, since their boundaries are connected by the conducting magnetic field lines. The data do not disagree with this assumption, since the southern hemisphere measurements tend to relate to the AE indices in the same way as the northern hemisphere measurements. However, there are cases where the potential measurements over the winter hemisphere seem to be less accurate than the summer measurements. It appears that the true locations of the polar cap auroral boundaries tend to be obscured by the erratic electric field fluctuations which are associated with low ionospheric conductivity, particularly in the late morning auroral zone. The increased errors in the winter is from the inability to easily identify the reversal boundary.

The electrojet currents and their indices are shown to be approximately proportional to the potential as predicted by Equation 14. There is a fair amount of spread to the data since the width and distribution of the electrojet current and the Hall conductivity are not constant. For a comparison between the data and theory, let us use values of solar radiation induced conductivity equal to 0 in the winter and 7 mhos in the summer. We need to add to this background conductivity (taking the square root of the sum of the squares), the conductivity induced by particle precipitation. According to Hardy *et al.* (1985) for K_p = 2 this induced conductivity is approximately 3 mho at 18 hours MLT and 10 mhos at 6 hours MLT. Therefore in the dusk electrojet the conductivity is approximately 3 mho in winter and 7.6 mho in summer, and the slopes on Figure 5 should be about 3.75 and 9.5 nt kV^{-1}. In the dawn electrojet the conductivity is about 10 mho in winter and 12.2 mhos in summer, and the slopes on Figure 6 should be about 12.5 and 15.2 nt kV^{-1}. We find that our 90% slopes which are given in Table 1 are not far from these values, but on the average the slopes are much less. Most likely this is due to the effects of the neutral winds, as discussed previously.

Due to these numerous other variables which we cannot control, the data show a large amount of "scatter" on the graphs. Nevertheless, there is sufficient order to enable us to fit the data to a curve. An equation which describes the relationship between the AE index and polar cap potential drop would have some utility, as mentioned in the Introduction.

We will concentrate on just the data shown in Figure 7, but first we will attempt to eliminate from the data base some of the satellite passes which did not pass through the full potential drop. It is well known that the plasma convection pattern tends to be rotated slightly clockwise (Heppner and Maynard,

FIG. 9. AE INDEX VS. POLAR CAP POTENTIAL FOR THE NORTHERN HEMISPHERE WINTER PERIOD, FOR THE CASES IN WHICH AN UNAMBIGUOUS SUBSTORM PHASE COULD BE IDENTIFIED. These data points were obtained during substorm (a) growth, (b) expansion, and (c) recovery stages.

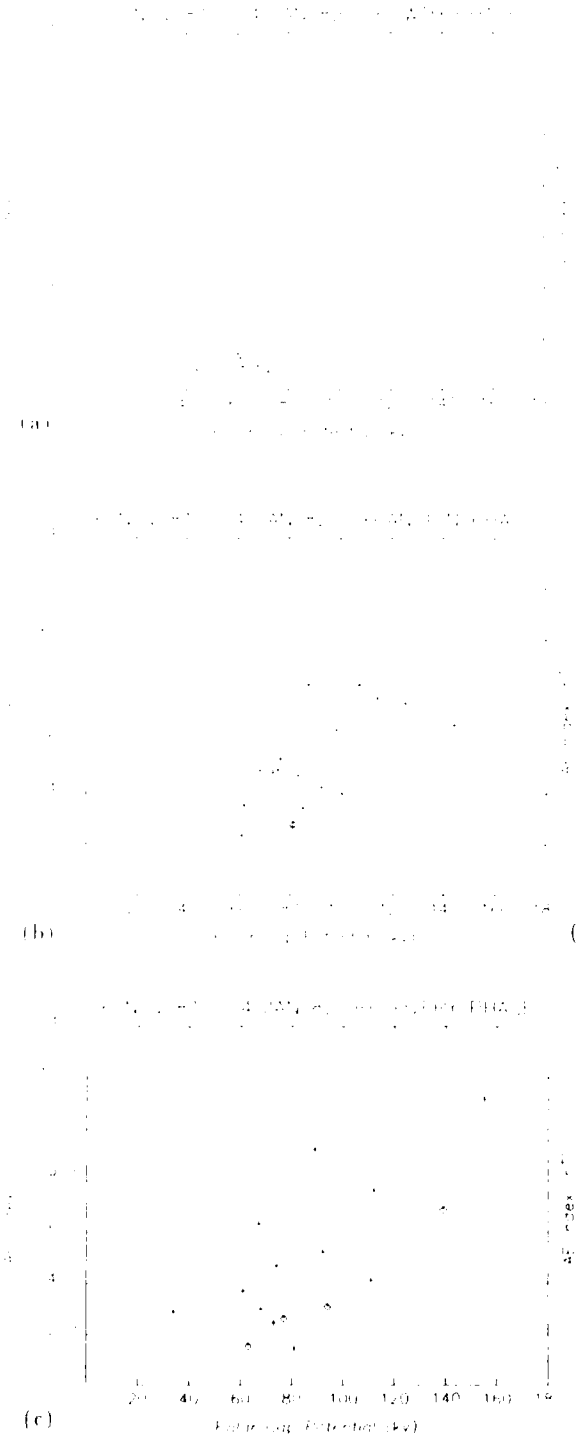

FIG. 10. AE INDEX VS. POLAR CAP POTENTIAL FOR THE NORTHERN HEMISPHERE SUMMER PERIOD, FOR THE CASES IN WHICH AN UNAMBIGUOUS SUBSTORM PHASE COULD BE IDENTIFIED. These data points were obtained during substorm (a) growth, (b) expansion, and (c) recovery stages.

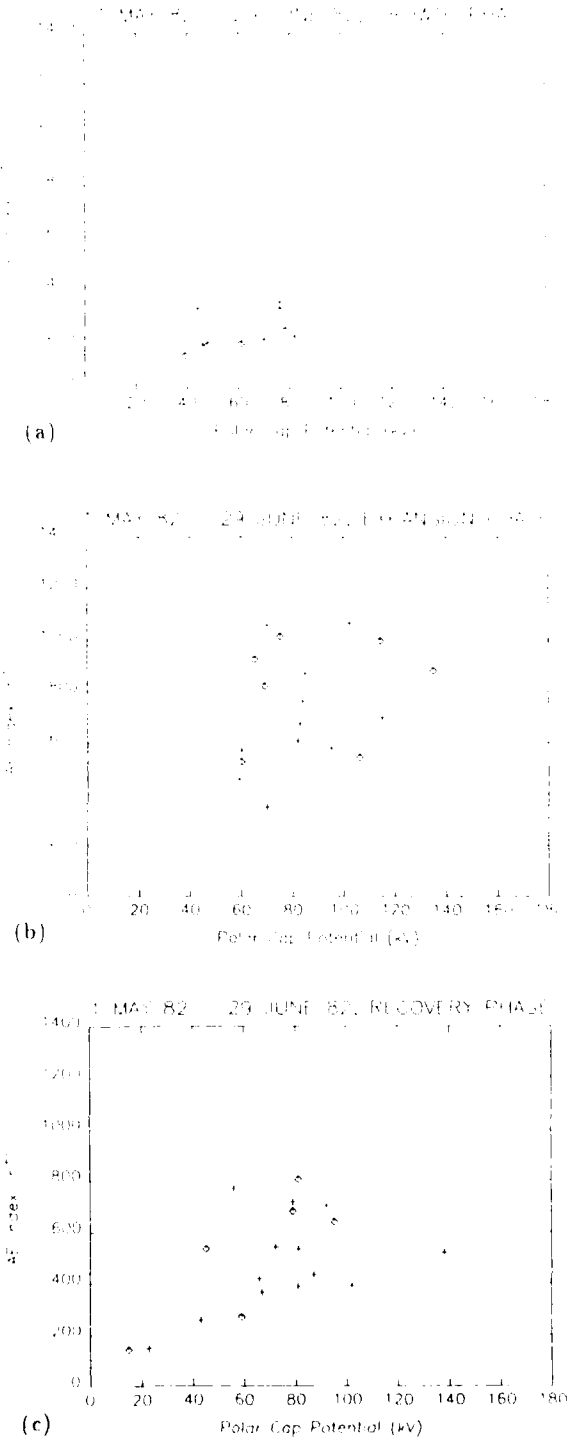

1987), and in Figure 6 it was found that some of the dawn potentials which were measured at MLT greater than 8 hours were obviously low. Therefore, we use just the orbits which passed through the dawn auroral zone at MLT less than 8 hours, and also passed through the dusk auroral zone at MLT less than 20 hours. This reduces the number of measurements from 309 to 211 cases in the winter time period, and from 218 to 129 cases in the summer time period.

Conventional least-square-error techniques could be used to determine the curve fits. However, these methods minimize the vertical error between the curve and the "dependent variable" data points, assuming that the "independent variable" on the horizontal axis has been measured with a much smaller error. A least-square-error fit with AE as the independent variable gives a result which is substantially different from the result which is obtained with Φ, the polar cap potential, as the independent variable. Rather than choosing either AE or Φ to be the independent variable, it is better to find the curve which *minimizes* the total square-error in both the vertical and horizontal directions simultaneously. We have used the "simplex" method for this purpose (specifically, a variation of the Amoeba subroutine by Press *et al.* (1986)), since it can minimize by trial-and-error any arbitrary function.

The results of fitting three different equations to the data are shown in Figure 11. The long-dashed lines on the graphs show the result of fitting the data to a straight line:

$$\mathrm{AE} = a + b\Phi \,. \tag{16}$$

But the data appear to have a non-linear trend. This can be expected, since the electrojet current depends on both the potential drop and the Hall conductivity, and precipitation-induced conductivity enhancements are related to the potential drop. Therefore, it is not unreasonable to test relationships with an exponent other than one. The other equations which have been fit to the data are: a power law,

$$\mathrm{AE} = a + b\Phi^c \,, \tag{17}$$

which are shown with the solid lines; and a second-order polynomial,

$$\mathrm{AE} = a + b\Phi + c\Phi^2 \,. \tag{18}$$

which are shown with the short-dashed lines. The values of the constants which were determined by these fits are given in Table 2. The total square-error, χ^2, and the standard deviation, σ, are also included in Table 2. The quantity χ^2 is minimized by the curve-fitting routine. It is defined for our purposes as:

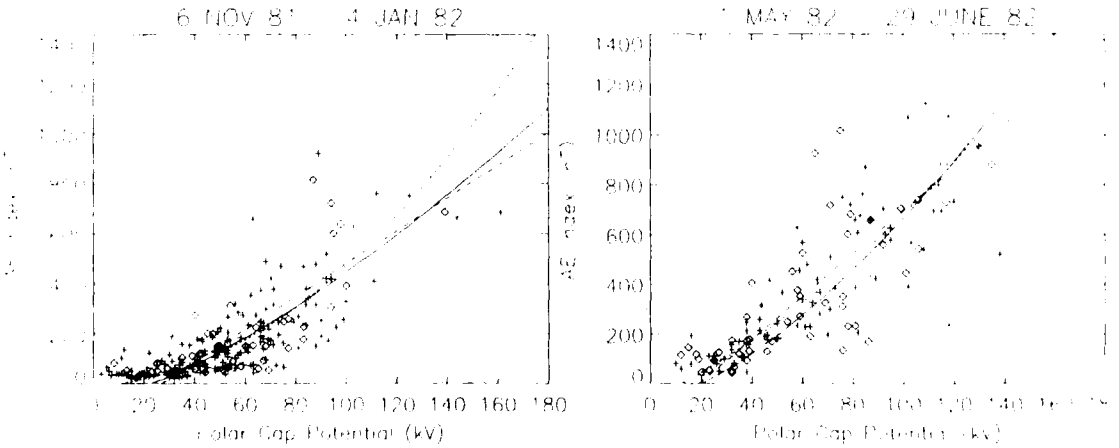

(a) (b)

FIG. 11. SCATTER PLOTS OF AE INDEX VS. POLAR CAP POTENTIAL AND THE RESULTS OF FITTING CURVES TO THE DATA. These data include only the satellite passes at MLT less than 8 hours in the dawn auroral zone and less than 20 hours in the dusk auroral zone. (a) Winter period in the northern hemisphere. (b) Summer period. The long-dashed lines show the fits of Equation 16, a straight line. The solid lines show the fits of Equation 17, a power law. The short-dashed lines show the fits of Equation 18, a second-order polynomial. The parameters for these lines are given in Table 2.

$$\chi^2 = \sum_{i=1}^{N}\left(\frac{AE_i - AE(\Phi_i)}{AE_{MAX}}\right)^2 + \sum_{i=1}^{N}\left(\frac{\Phi_i - \Phi(AE_i)}{\Phi_{MAX}}\right)^2 . \quad (19)$$

Note that the AE and Φ errors have been normalized to dimensionless quantities by dividing by their maximum values. We have used 1400 nT and 180 kV, the maximum values on the plot scales. The standard deviation is calculated as:

$$\sigma = \sqrt{\frac{\chi^2}{2N}} . \quad (20)$$

These quantities have some similarities to the conventional definitions, but there are differences.

The power-law formula has the best fit to the data in Figure 11a, the winter data, and the second-order polynomial has the lowest error in Figure 11b, the summer data. However, there is not a very large difference in the errors. The standard deviations for the non-linear fits are not significantly different from those for the straight line, so the straight lines seem to be sufficient for modeling the data.

By inverting Equation 16 and using the values given in Table 2 for a and b, it is found that $\Phi(kV) = 26.8 + 0.152AE(nT)$ in the winter and $\Phi(kV) = 19.2 + 0.116AE(nT)$ in the summer. These results are similar to those found by Reiff *et al.* (1981) ($\Phi(kV) = 41 + 0.11AE(nT)$), Ahn *et al.* (1984) ($\Phi(kV) = 36 + 0.089AE(nT)$), and by Richmond *et al.* (1990) ($\Phi(kV) = 22 + 0.119AE(nT)$).

One problem with these equations is that they give nonsensical results for AE at very low potentials. The earlier studies had very little data with polar cap potentials below 30 kV, and our own data show that AE is very low when the potential is below this value. This is not too surprising, since the auroral zones may be contracted to a position northward of the magnetometer stations when the convection is weak. Additionally, the low potentials will usually be associated with northward IMF B_Z conditions, with erratic convection patterns (Heppner and Maynard, 1987) and disorganized electrojet currents.

Considering that Ahn *et al.* (1984) and Richmond *et al.* (1990) had used ground-based measurements and computer algorithms to calculate the polar cap potential drops, it is remarkable that their results are in such close agreement with these obtained by *in situ* satellite measurements. This indicates that the Kamide method is fairly accurate. In another paper Ahn *et al.* (1989) had also used the magnetogram inversion technique, and where both AE indices and calculated polar cap potentials were given their data points from the month of July fit within the spread of our points in Figure 7b. They had points at (81 kV, 562 nT) and (66 kV, 142 nT) before substorms and at (81 kV, 1062 nT) and (109 kV, 800 nT) just after substorm maximum phase (the last AE value was estimated from a graph rather than given in the text). Since these points have a spread similar to ours, it appears that the scatter in the plots is more an inherent property of the potential-AE relation than a problem with our satellite sampling.

Figures 5, 6, and 7 have trends which indicate that the ionospheric conductivity increases as the polar cap potential increases, since the AE indices increase more rapidly (i.e., the slope is greater) as the potential increases. This enhanced conductivity is due to electron precipitation associated with field-aligned currents. The change in the slope is much more noticeable in AL than it is in AU, which is consistent with the conductivity in the dawn auroral zone increasing much more than in the dusk auroral zone as magnetic activity increases (Hardy *et al.*, 1987). The conductivity enhancements cause an apparent discontinuity in the AE-potential relations in Figure 7, occurring at about 60 kV in the winter and 40 kV in the summer. This difference between the seasons is curious. One possible explanation is

TABLE 2. RESULTS OF THE CURVE FITS SHOWN ON FIGURES 11A (winter) AND 11B (summer).

Season	Equation	a	b	c	χ^2	σ
winter	16	176	6.56	—	3.942	0.0967
	17	65.	0.79	1.40	3.255	0.0878
	18	8.	0.45	0.044	3.351	0.0891
summer	16	165.	8.60	—	3.536	0.1171
	17	69.	0.81	1.48	3.550	0.1173
	18	67.	5.13	0.024	3.447	0.1156

that, due to the greater solar-induced conductivity in the summer, for a given potential the Pedersen and field-aligned currents in the summer hemisphere are greater than in the winter hemisphere. Therefore, at a given potential the particle precipitation and the precipitation-induced conductivity will also be greater in the summer hemisphere.

Much of the scatter in these data is due to the dynamics of magnetospheric substorms. In fact, since substorms may be due to an "unloading" of stored energy from the magnetotail (Akasofu, 1989) there may be times when substorms occur while the polar cap potential (which is controlled by the IMF) is nearly constant. Therefore we should expect that at some potentials the AE indices will have a wide range, due to enhanced electrojet currents during substorms. The role of substorms is evident in Figures 9 and 10. Wherever a substorm growth phase has been identified the AE indices are down near the lower 10% curve; during substorm expansion phase the AE indices move upward toward the 90% curve; and during the recovery phase the AE indices, and sometimes the polar cap potential, start to move downward.

Kan *et al.* (1988) have proposed that the polar cap potential must reach a certain critical level (70 kV in their model) in order for substorm onset to occur. Our results tend to support that aspect of their theory. Figure 7 shows that below approximately 60 kV the AE indices tend to remain low, with little vertical scatter, but above 60 kV the AE indices become large and widely scattered, indicative of substorm activity. Figures 9 and 10 are even more convincing: the potentials during the growth phase are between 40 and 80 kV and the potentials during substorm expansion are above 60 kV. During substorm recovery several of the measured potentials are below 80 kV, but there are also instances where the potentials are still high. According to the Kan *et al.* (1988) model, substorm recovery occurs when either the polar cap potential drops below the critical level or the diffuse auroral conductance belt moves equatorward from the convection reversal.

4. CONCLUSION

We have shown that the AU, AL, and AE indices can be related to the respective dusk auroral, dawn auroral, and polar cap potentials. Due to the large number of variables the relationships are approximate rather than exact. Linear relationships which indicate the bounds of 80% of the data points and median slopes are specified. Different parameters are required in order to bracket the data at different times of the year. Since the AE indices are measured only in one hemisphere, these indices are greater during the local summer, when the ionospheric conductivity is greater than in the winter.

At very low polar cap potentials the AE measurements do not appear to be very accurate, due to the movement of the auroral oval northward, away from the magnetometer stations. At high potentials the electrojet currents are influenced by precipitation-induced conductivity enhancements. The enhanced conductivities are more noticeable in the AL index than in the AU index, since the westward electrojet is associated with upward current and precipitating electrons while the eastward electrojet is associated with downward current.

Our data are consistent with the prior observations of Kamide and Baumjohann (1985), Ahn *et al.* (1989), and many others that the increase in the electrojet current intensity prior to substorm onsets is due to an increase in the electric field/potential, and conductivity enhancements after onsets contribute to the substorm currents. We also find that substorms appear to occur when the polar cap potential exceeds a threshold of approximately 60 kV, which supports (but does not necessarily prove) a theory by Kan *et al.* (1988) for the cause of substorm onsets.

Although the AE-potential graphs do have a lot of "scatter", there is sufficient order to the data to derive a least squares fit equation. By inverting the equation it is possible to derive reasonable estimates for the potentials from the AE indices. This would be a logical option whenever an estimate of the polar cap potential is required for a specific time period for which AE is known. Although the AE indices do have faults (Akasofu, 1989) they are more accurate than K_p for indicating the state of the magnetosphere-ionosphere system at a given moment. Future modelers of ionospheric convection, conductivities, currents, precipitation, and Joule heating should index their models to AE rather than K_p.

Seasonal effects also need to be taken into consideration more frequently than they have in the past. In other words, most people who have used the AE index in one way or another have done so with little regard for the time of the year. It could be useful to have yet another index, similar to AE, but with adjustments made for annual variations.

Acknowledgements - We thank T. Iyemori at Kyoto University for providing the high-resolution AE indices. The research at Regis College was supported by the Air Force Geophysics Laboratory through contract F19628-86-K-0045. Work at the Geophysics Laboratory was supported by NASA/GSFC, and by AFOSR through task 2311G5. Work at ST Systems was supported under contract to NASA/GSFC. This research benefited from use of the NASA Space Physics Analysis Network (SPAN).

REFERENCES

Ahn, B.-H., R. M. Robinson, Y. Kamide, and S.-I. Akasofu (1983) Electric conductivities, electric fields and auroral particle energy injection rate in the auroral ionosphere and their empirical relations to the horizontal magnetic disturbances. *Plant. Space Sci.* **31**, 641.

Ahn, B.-H., S.-I. Akasofu, Y. Kamide, and J. H. King (1984) Cross-polar cap potential drop and the energy coupling function. *J. Geophys. Res.* **89**, 11028.

Ahn, B.-H., H. W. Kroehl, Y. Kamide, and D. J. Gorney (1989) Estimation of ionospheric electrodynamic parameters using ionospheric conductance deduced from Bremsstrahlung X ray image data. *J. Geophys. Res.* **94**, 2565.

Akasofu, S.-I. (1989) Future of magnetospheric substorm-storm research. *Eos, Transactions, American Geophysical Union* **70**, 529.

Allen, J. H., and H. W. Kroëhl (1975) Spatial and temporal distributions of magnetic effects of auroral electrojets as derived from AE indices. *J. Geophys. Res.* **80**, 3667.

Baker, D. N., E. W. Hones, J. B. Payne, and W. C. Feldman (1981) A high time resolution study of interplanetary parameter correlations with AE. *Geophys. Res. Lett.* **8**, 179.

Bargatze, L. F., D. N. Baker, R. L. McPerron, and E. W Hones (1985) Magnetospheric impulse response for many levels of geomagnetic activity. *J. Geophys. Res.* **90**, 6387.

Baumjohann, W. and Y. Kamide (1984) Hemispherical Joule heating and the AE indices. *J. Geophys. Res.* **89**, 383.

Berthelier, A. (1976) Influence of the polarity of the interplanetary magnetic field on the annual and the diurnal variations of magnetic activity. *J. Geophys. Res.* **81**, 4546.

Burch, J. L. (1973) Effects of interplanetary magnetic sector structure on auroral zone and polar cap magnetic activity. *J. Geophys. Res.* **78**, 1047.

Crooker, N. U. and G. L. Siscoe (1981) Birkeland currents as the cause of the low-latitude asymmetric disturbance field. *J. Geophys. Res.* **86**, 11201.

Davis, T. N., and M. Sugiura (1966) Auroral Electrojet activity index AE and its Universal Time variations. *J. Geophys. Res.* **71**, 785.

Doyle, M. A. and W. J. Burke (1983) S3-3 measurements of the polar cap potential. *J. Geophys. Res.* **88**, 9125.

Foster, J. C., J. M. Holt, R. C. Musgrove, and D. S. Evans (1986) Ionospheric convection associated with discrete levels of particle precipitation. *Geophys. Res. Lett.* **13**, 656.

Foster, J. C., T. Fuller-Rowell, and D. S. Evans (1989) Quantitative patterns of large-scale field-aligned currents in the auroral ionosphere. *J. Geophys. Res.* **94**, 2555.

Hardy, D. A., M. S. Gussenhoven, R. Raistrick, and W. J. McNeil (1987) Statistical and functional representations of the patterns of auroral energy flux, number flux, and conductivity. *J. Geophys. Res.* **92**, 12275.

Heppner, J. P. and N. C. Maynard (1987) Empirical high-latitude electric field models. *J. Geophys. Res.* **92**, 4467.

Kamide, Y. and W. Baumjohann (1985) Estimation of electric fields and currents form international magnetospheric study magnetometer data for the CDAW 6 intervals: implications for substorm dynamics. *J. Geophys. Res.* **90**, 1305.

Kan, J. R., L. Zhu, and S.-I. Akasofu (1988) A theory of substorms: onset and subsidence. *J. Geophys. Res.* **93**, 5624.

Killeen, T. L., P. B. Hays, G. R. Carignan, R. A. Heelis, W. B. Hanson, N. W. Spencer, and L. H. Brace (1984) Ion-neutral coupling in the high-latitude F region: evaluation of ion heating terms from Dynamics Explorer 2. *J. Geophys. Res.* **89**, 7495.

Lyons, L. R. and R. L. Walterscheid (1986) Feedback between neutral winds and auroral arc electrodynamics. *J. Geophys. Res.* **91**, 13506.

Mayaud, P. N. (1980) *Derivation, meaning, and use of geomagnetic indices*, Geophysical monograph 22, American Geophysical Union, Washington, DC.

Maynard, N. C., E. A. Bielecki, and H. F. Burdick (1981) Instrumentation for vector electric field measurements from DE-B. *Space Sci. Instrum.* **5**, 523.

Meng, C.-I. and S.-I. Akasofu (1968) Polar magnetic substorms in the conjugate areas. *Radio Sci.* **3**, 751.

Meng, C.-I., B. Tsurutani, K. Kawasaki, and S.-I. Akasofu (1973) Cross- correlation analysis of the AE index and the interplanetary magnetic field Bz component. *J. Geophys. Res.* **78**, 617.

Nisbet, J. S. (1982) Relations between the Birkeland currents, the auroral electrojet indices and high latitude Joule heating. *J. Atm. Terr. Phys.* **44**, 797.

Perrault, P. and S.-I. Akasofu (1978) A study of geomagnetic storms. *Geophys. J. R. Astron. Soc.* **54**, 547.

Press, W. H., B. P. Flannery, S. A. Teukolsky, and W. T. Vetterling (1986) *Numerical recipes: the art of scientific computing*, Cambridge University Press, New York.

Reiff, P. H., R. W. Spiro, and T. W. Hill (1981) Dependence of polar cap potential drop on interplanetary parameters. *J. Geophys. Res.* **86**, 7639.

Rich, F. J. and N. C. Maynard (1989) Consequences of using simple analytical functions for the high-latitude convection electric field. *J. Geophys. Res.* **94**, 3687.

Richmond, A. D., Y. Kamide, S.-I. Akasofu, D. Alcaydé, M. Blanc, O. de la Beaujardière, D. S. Evans, J. C. Foster, E. Friis-Christensen, J. M. Holt, R. J. Pellinen, C. Senior, and A. N. Zaitzev (1990) Global measures of ionospheric electrodynamic activity inferred from combined incoherent scatter radar and ground magnetometer observations. *J. Geophys. Res.* **95**, 1061.

Sauvaud, J. A., J. P. Treilhou, A. Saint-Marc, J. Dandouras, H. Reme, A. Korth, G. Kremser, G. K. Parks, A. N. Zaitzev, V. Petrov, L. Lazutine, and R. Pellinen (1987) Large scale response of the magnetosphere to a southward turning of the interplanetary magnetic field. *J. Geophys. Res.* **92**, 2365.

Spiro, R. W., P. H. Reiff, and L. J. Maher, Jr. (1982) Precipitating electron energy flux and auroral zone conductances - an empirical model. *J. Geophys. Res* **87**, 8215.

Tsurutani, B. T., J. A. Slavin, Y. Kamide, R. D. Zwickl, J. H. King, and C. T. Russell (1985) Coupling between the solar wind and the magnetosphere: CDAW 6. *J. Geophys. Res.* **90**, 1191.

Wygant, J. R., R. B. Torbert, and F. S. Mozer (1983) Comparison of S3-3 polar cap potential drops with the interplanetary magnetic field and models of magnetopause reconnection. *J. Geophys. Res.* **88**, 5727.